Quantifying the affinity difference between lithium and close identity ions using ETS-10 titanosilicate

Winters Kexi Guo¹, Emma Rosko¹, Grant Zeszutek¹, Uriahe DeVore¹, Xueyi Zhang¹, Michael J. Janik¹, Gina Noh¹*

¹ Department of Chemical Engineering, Pennsylvania State University, University Park, PA, 16802 USA

* Corresponding author: gnoh@psu.edu

Abstract

The affinity difference between lithium and potassium ions for adsorption to a titanosilicate adsorbent is quantified. Experimental and computational methods examine the thermodynamics of Na⁺-K⁺ and Na⁺-Li⁺ ion exchange from dilute aqueous solution using modified ETS-10 titanosilicate. Equilibrium uptake data were analyzed with a modified Langmuir isotherm that accounts for ion exchange involving the desorption of Na⁺ from the modified ETS-10 framework together with adsorption of Li⁺ or K⁺ to the framework. The equilibrium constant for ion exchange of Na⁺ from modified ETS-10 framework with K⁺ from aqueous solution is 6-fold greater than the equilibrium constant for Li⁺ exchange. This affinity difference is supported by density functional theory (DFT) calculations of ion affinity to the modified ETS-10 framework. Energy differences from DFT were interpreted using a thermochemical cycle to account for hydration and solvation of cations, thus enabling comparison between experiment and theory. DFT-derived energy differences also revealed the binding affinity difference of the various sites of ETS-10 among Li⁺, Na⁺, and K⁺.

1. Introduction

Lithium is critically important for state-of-the-art renewable energy technologies, including batteries, and demand for this element is projected to increase fivefold over the next decade [1-4]. Current production methods separate lithium from impurities such as potassium using solvent extraction processes that

demand substantial energy inputs and utilize large quantities of hazardous organic solvents [5,6]. As a result, sustainable and green chemistry principles have guided investigations into alternate separation methods, with continuous ion exchange (CIX) and continuous ion chromatography (CIC) showing particular promise in initial studies [7-12]. Commonly used ion exchangers, such as zeolite X, have demonstrated high selectivity for certain precious metal such as Ag. However, their low capacity is a common issue [13-15].

One promising ion exchange solid is titanosilicate ETS-10, a 1-dimensional large pore (12-membered rings, 7.6 Å × 4.9 Å) microporous material composed of SiO₄ tetrahedral units and octahedral TiO₆ units [16-18]. ETS-10 has previously demonstrated high ion exchange capacity (1.31 mmol g⁻¹ for Pb²⁺) for heavy metals in wastewater treatment. [19-21] This high capacity reflects the charge density of this microporous titanosilicate, which arises from the continuous "chains" of octahedral TiO₆ units that require 2 charge-balancing monovalent ions per Ti [16,17]. Following a typical synthesis approach, each ETS-10 unit cell (Ti₁₆Si₈₀O₂₀₈³²⁻) contains 24 Na⁺ and 8 K⁺ occupying five symmetry inequivalent groups of ion exchange sites (Figure 1) [16,17]. Such configuration results in ETS-10 possessing a high surface charge density of -12.49 μ C cm⁻², which is significantly higher than that of some traditional zeolite ion exchangers such as EMT (-0.05 μ C cm⁻²) and FAU (-0.06 μ C cm⁻²) [21,22]. This unique property of ETS-10 may enable it to exhibit a high ion exchange capacity.

ETS-10 has been extensively investigated for ion exchange applications with heavy metal ions, rare earth element ions, and radioactive ions [19-21, 23-26]. To our knowledge, there are limited studies on the ion exchange of lithium and its close identity impurities using ETS-10, as well as the investigation of ion exchange using density functional theory (DFT) calculations. In this paper, we investigate the equilibrium of ETS-10 ion exchange with various ions. We first consider high concentration ion exchange, examine the extent to which ETS-10 can be stable and approach to a single alkali-exchange form. We verified the ion occupancy of high concentration ion exchange results using ²³Na 2D 3Q MAS

NMR spectroscopy and DFT calculations. Then we quantified the exchange affinity of Li⁺ and K⁺ with modified ETS-10 from dilute aqueous solution and supported by DFT calculations.

This work aims to provide insights into the separation of lithium from close identity impurities that are commonly found in lithium sources. Furthermore, we aim to demonstrate the utility of DFT in studying ion exchange process and enhancing our understanding on porous materials. Our findings can contribute to the development of more efficient and selective separation techniques for lithium, addressing an important challenge in the field.

2. Experimental Methods

- **2.1. Chemicals**. The following chemicals were used as received, without further purification: NaOH (EMD Millipore, ≥99%), KOH (EMD Millipore, ≥84%), TiO₂ (Acros Organics, P25), sodium silicate solution (Merck, Na₂O (7.5–8.5%), SiO₂ (25.5–28.5%), pH 11-11.5), HCl solution (Sigma-Aldrich, 37 wt %), LiNO₃ (Acros Organics, 99.999%), NaNO₃ (Acros Organics, 99%), and KNO₃ (Acros Organics, 99%). Unless otherwise noted, deionized water (resistivity ≤ 18.2 MΩ·cm) was used. Y, Li, Na, and K standards (1000 ppm certified reference in 0.1% v/v HNO₃) from Inorganic Ventures were used for ICP-OES measurements.
- **2.2. Synthesis of ETS-10 and "washed" ETS-10.** Phase-pure ETS-10 was synthesized following previously reported protocols [23]. Briefly, aqueous solutions of NaOH (7.9 M, 6.0 g) and KOH (7.6 M, 6.5 g) and a slurry of TiO₂ (0.80 g of solid in 4.0 mL water) were prepared separately then added dropwise to a stirring sodium silicate solution (12.2 g; 500 rpm; ambient temperature) in a fluorinated ethylene propylene (FEP) bottle (125 mL). The pH of the mixture was adjusted to 10.5 by dropwise addition of HCl solution (~6.9 g). The resulting synthesis gel had the molar ratios 3.4Na₂O: 1.5K₂O: 1TiO₂: 5.5SiO₂: xHCl: (116.7 + 3.45x) H₂O, where x=6.6-8.1. The gel was agitated in the FEP bottle using an orbital shaker (200 rpm) for 0.5 h then transferred to a Teflon liner (45 mL), which was sealed into an autoclave vessel (45 mL, Parr Instrument Company) then heated to 503 K for 72 hours. The

mixture was transferred from the Teflon liner and centrifuged (4500 rpm, 0.33 h), then the supernatant was decanted. The solids were combined with water and centrifuged (4500 rpm, 0.33 h), with the supernatant decanted. This process was repeated until the supernatant pH was ~10. Solids were then collected and dried at 343 K overnight.

As synthesized ETS-10 was treated by contacting with 0.5 M aqueous solutions of KNO₃, NaNO₃, or LiNO₃ (0.1 L g⁻¹_{solid}) at room temperature for 2 h (stirring \sim 500 rpm). The slurries were centrifuged (4500 rpm, 0.33 h), with the supernatant decanted. This procedure was repeated three times, for a total of four washes. The solids were subsequently rinsed by combining with water (0.2 L g⁻¹_{solid}), until the supernatant conductivity decreased below 50 mS/cm. Solids were collected (mixture was centrifuged at 4500 rpm for 0.33 h, the supernatant was decanted) and dried at 343 K overnight. KNO₃, NaNO₃, and LiNO₃-washed ETS-10 samples are denoted as K-, Na-, and Li-ETS-10, respectively.

Concentrations of K, Na, and Li in aqueous solution samples before and after ion exchange were measured using ICP-OES (Agilent ICP-OES 700 series). Samples with concentrations greater than the calibration curve range were diluted, with dilution factors between 1.1-3, while all other samples were used neat. To each sample (10 mL aliquot) was added internal standard Y (0.2 mL; 1000 ppm certified reference in 0.1% v/v HNO₃; Inorganic Ventures) and concentrated HNO₃ (0.01 mL). The following wavelengths were selected for each element: Li 670.73 nm, Na 589.592 nm, K 769.897 nm, and Y

377.433 nm. Linear calibration curves were obtained using standard solutions of 0-100 ppm Li (1000 ppm certified reference in 0.1% v/v HNO₃), 0-200 ppm K (1000 ppm certified reference in 0.1% v/v HNO₃), and 0-200 ppm Na (1000 ppm certified reference in 0.1% v/v HNO₃), with internal standard Y. Samples were analyzed in random order to minimize systematic error. Five replicates of each sample were analyzed, and the average of their values is reported.

- 2.4. Characterization. As-synthesized and washed ETS-10 samples were analyzed using powder X-ray diffraction (pXRD) with Ni-filtered Cu K α radiation (λ = 1.54 Å) at 40 mA and 45 kV on a PANalytical Empryean diffractometer. K, Na, Li, Ti, and Si contents of solid K-, Na-, and Li-ETS-10 and assynthesized ETS-10 were determined by ICP-AES (Galbraith Laboratories, Inc.; solids were digested using HCl, HNO₃, and HF). Single- and triple-quantum ²³Na MAS NMR spectra were recorded at 132.25 MHz on a Bruker Avance III HD spectrometer. Samples were loaded into 4.0 mm zirconia rotors spun at 10 kHz. The pulse program "mp3qzqf" (Bruker Advance) was used with a recycling delay of 0.5 s. Spectra were sheared and analyzed using Bruker Topspin. Chemical shift (ppm) scales are referenced to v_0 and $3v_0$ in the F2 and F1 dimensions, respectively. Diffuse reflectance UV-vis spectra for solid samples were measured at room temperature using a Shimadzu UV-2600 spectrometer (220-450 nm, 0.1 nm resolution, ~4 nm min⁻¹ scan rate) equipped with an ISR-2600Plus integrating sphere attachment. BaSO₄ was used as the reference material.
- 2.5. Modified Langmuir model for quantifying exchange affinity. Quantifying Na-ETS-10 exchange capacity and exchange equilibrium for different ions is essential to assess its suitability for use as an ion exchange solid. A Langmuir adsorption model is commonly used to determine the exchange capacity and equilibrium, but this model only considers the adsorption step of the ion exchange reaction. Here, the Langmuir adsorption isotherm expression is modified to reflect the entire ion exchange reaction.

The overall ion exchange reaction with equilibrium constant $K_{A,M}$ (Eq. 1a) can be written as the initial desorption of M from the framework, FW (M_n -FW, where n represents the total ions adsorbed to

the framework) to generate a vacancy * and an aqueous M⁺ ion (Eq. 1b). In the second step, aqueous A⁺ adsorbs to the vacant site (Eq. 1c).

$$M_n - FW + A^+(aq) \stackrel{K_{A,M}}{\longleftrightarrow} A/M_{n-1} - FW + M^+(aq)$$
 Equation 1a
 $M_n - FW \rightarrow */M_{n-1} - FW^- + M^+(aq)$ Equation 1b
 $*/M_{n-1} - FW^- + A^+(aq) \rightarrow A/M_{n-1} - FW$ Equation 1c

The overall reaction (Eq. 1a), taken together with a site balance, can be used to define $K_{A,M}$ as:

$$K_{A,M} = \frac{\theta \cdot C_{M,e}}{(1-\theta) \cdot C_{A,e}}$$
 Equation 2a

where $C_{M,e}$ and $C_{A,e}$ represent equilibrium aqueous phase concentration of species M^+ and A^+ , respectively, and θ is the fractional site coverage by ion A, given by:

$$\theta = \frac{Q_{A,e}}{Q_{A,max}}$$
 Equation 2b

where $Q_{A,e}$ is the equilibrium sorbent phase concentration of A, and $Q_{A,max}$ is the maximum concentration of A that can be adsorbed to the sorbent.

Combining Equations 2a and 2b yields:

$$K_{A,M} = \frac{Q_{A,e} \cdot C_{M,e}}{(Q_{A,max} - Q_{A,e}) \cdot C_{A,e}}$$
 Equation 3

 $Q_{A,e}$ can be determined from mole balance to be the difference between $C_{A,i}$, the initial concentration of ion A, and $C_{A,e}$, normalized by the mass of solid. Equation 3 is used to fit experimental concentration data to obtain numerical values for $K_{A,M}$ and $Q_{A,max}$

This modified Langmuir expression has similar assumptions to the Langmuir adsorption isotherm: (1) the solution behaves thermodynamically ideally; (2) exchange sites are identical, and adsorbed ions do not interact; and (3) each adsorption site can hold at most one ion, preventing multi-

layer adsorption [27]. These assumptions are reasonable for the experimental conditions presented in this work. Ion exchange isotherms are measured at low ion concentrations, and < 20% of possible exchange sites participate in ion exchange.

2.6. Computational methods. Density functional theory methods were used to calculate the energy change associated with ion exchange reactions. All DFT calculations were carried out using the Vienna ab initio simulation package (VASP), version 5.4.1 [28]. VASP is a periodic plane-wave basis set code that allows the representation of extended electronic structure of the solid [29]. The electron exchange and correlation energies were computed using the Perdew, Burke, and Ernzehof version of the generalized gradient approximation (GGA) functional [30]. The projector augmented-wave (PAW) [31] method was used to represent the ion-core electron interactions. The plane-wave basis set cutoff energy was set to 450 eV. Convergence of ΔE values with respect to ENCUT was confirmed to within 0.02 eV across 8 different ion exchange energies. The following were treated as valence electrons: Li 1s and 2s; Na 2s and 2p; K 3s and 3p; Ti 3d and 4s; O 2s and 2p; and Si 3s and 3p.

The ETS-10 framework structure was taken from the International Crystal Structure Database, which was based on the work of Anderson et al. [16]. Cations were incorporated onto the framework according to site occupancies reported by Anderson et al. [32]. Subsequently, both the atom positions and unit cell dimensions were optimized, being considered converged when total energy changed by < 0.001 eV.

The ion exchange energy (ΔE) of Na-ETS-10 with Li⁺ and K⁺ was calculated using:

$$\Delta E = E_{A/Na-ETS-10} + E_{Na^+} - E_{Na-ETS-10} - E_{A^+}$$
 Equation 4

where $E_{\text{A/Na-ETS-10}}$ is the energy of Na-ETS-10 with one A ion (Li⁺ or K⁺) on the framework; $E_{\text{Na-ETS-10}}$ is the energy of Na-ETS-10; and E_{Na^+} and E_{A^+} are the energies of aqueous Na⁺ and A⁺ which are approximated using two different approaches (see details in Section 3.3).

All DFT calculations consider neutral systems in which the -32 charge of the framework unit cell is compensated by 32 alkali cations. All ETS-10 DFT models include only framework alkali charge compensating cations and do not explicitly include water. We expect that water molecules would be present in the pores of ETS-10 throughout the experiments conducted, and the omission of water in the DFT model is likely the main source of quantitative disagreement between DFT exchange energies and experimental observed exchange equilibrium constants. Despite this approximation in the models used, the DFT results show strong qualitative agreement with site preferences observed experimentally for the different alkali cations, as well as with trends in ion exchange favorability.

3. Results and Discussion

3.1. Structural properties of ETS-10 and its post-synthetically washed analogs

As-synthesized ETS-10 and A-ETS-10 (A = Li, Na, or K, where this nomenclature indicates ETS-10 materials that have been washed post-synthetically with aqueous solutions of cation A; Table 1) are characterized to assess their structural and chemical properties. Figure 2 shows diffractograms for ETS-10 and A-ETS-10 [33]. The diffractogram for as-synthesized ETS-10 shows the expected reflections for ETS-10 polymorph A (Fig. 2), with minor features associated with polymorph B consistent with previous reports of such intergrowths [16,17,32]. Reflections for quartz, anatase and rutile TiO₂, and ETS-4 (Supporting Information, Figure S1 shows simulated patterns for these materials), the common impurity phases for ETS-10 [17,34], are not observed. Taken together with elemental analysis of the solid material that indicate the expected Si/Ti stoichiometry for ETS-10 phase materials (Table 1, Si/Ti ~ 4.99), these data demonstrate the phase-purity of this ETS-10 material.

The diffractograms for A-ETS-10 materials (Fig. 2) are nearly identical to that for the assynthesized material, with no observed shifts in reflections, indicating that the post-synthetic washing procedure for high concentration cation exchange did not lead to detectable changes in unit cell parameters or phase or disruption of crystallographic long range order. The Si/Ti ratios are ~5 for all A-ETS-10 (Table

1). However, while cation density for ETS-10 and Na-ETS-10 have the expected values (~32 M/u.c., Table 1), these values are slightly smaller for both K- and Li-ETS-10 (30 and 29 M/u.c., respectively; Table 1) and suggest that H⁺ may also act as charge-balancing counterions for K- and Li-ETS-10. These ~2-3 H⁺/u.c. concentrations are unlikely to perturb the structure, as pore shrinkage and disruption of the continuous Ti-O-Ti chains was only observed at very low M/u.c. ratios [20,35]. The crystal habit and crystal size of assynthesized and A-ETS-10 materials are similar from scanning electron micrographs (Figure S4).

The structural integrity of the continuous Ti-O-Ti chains was assessed using UV-vis spectroscopy. The diffuse reflectance UV-vis spectrum for ETS-10 (Fig. 3) shows an adsorption band at ~282 nm. This transition reflects the bandgap of a TiO₂-based chain that is confined within an insulating SiO₂ matrix [36,37]. As a result, its presence can be taken as an indication of the structural integrity of the continuous Ti-O-Ti chains [37]. The spectra for A-ETS-10 (Fig. 3) are similar to that for ETS-10, each with an adsorption band at ~282 nm, despite cation densities < 32 M/u.c. for both K- and Li-ETS-10 (Table 1). Thus, as-synthesized ETS-10 and all A-ETS-10 materials maintain their phase and structural integrity.

As the washing treatments require higher cation concentrations than isotherm experiments, we take the results reported in this section to also confirm ETS-10 structural integrity will remain after ion exchange under dilute condition. Next, we examine the specific distribution of cations at ion-exchange sites within A-ETS-10 using a combined experimental and computational approach.

3.2. Compositional and structural stability of ion-exchanged Li, Na, K-ETS-10

Ion exchange sites in ETS-10 can be divided into five symmetry non-equivalent groups, with Groups I to III having 8 sites per unit cell (occupied by 24 Na ions in as-synthesized ETS-10) and Group IV and V have 4 sites each (occupied by 8 K ions in as-synthesized ETS-10) [17,32]. The distribution of cations in A-ETS-10 among these groups provides information about which ion-exchange sites will participate in low concentration ion exchange. Elemental analysis and ²³Na 2D 3Q MAS NMR spectra are

used to determine site occupation of cations in Li, Na, and K-ETS-10. DFT calculations consider the relative energy with varying site occupation to further corroborate site occupancy.

Elemental analysis (Table 1) of Na-ETS-10 indicates that Na and K occupy 28 and 4 ion-exchange sites (per unit cell), respectively. The locations of these Na cations were elucidated using nuclear magnetic resonance spectroscopy. The 23 Na 2D 3Q MAS NMR spectrum for Na-ETS-10 (Fig. 4) shows two features (δ = -15, -14 ppm and -12, -6 ppm) that indicate the presence of Na cations in Group I, II, III, and V sites, assigned according to previous work [32]. Notably, the spectrum lacks a high-field shoulder in the triple quantum axis, a feature that has been assigned to Na cations in Group IV sites [32]. These results together indicate that the 4 K cations occupy Group IV sites, while the remaining sites (Groups I-III and V) are occupied by Na cations.

These assignments were further examined using DFT-derived energies of possible Na-ETS-10 structures. Examined cation arrangements populated all sites of the same group with the same alkali metal cations (e.g., 8 Na cations in Group I sites) and matched experimentally measured cation stoichiometries (detailed in Table 2). Structures for K- and Li-ETS-10, discussed next in this section, considered all groups to be fully occupied with the same cation due to long range order and symmetry of the structure, despite slight differences from experimental compositions, as mixed occupancy of ion exchange groups is not observed from as-synthesized ETS-10 and modified ETS-10 [17,32]. For Na-ETS-10, two possible structures were examined: 4 K⁺ per unit cell occupied either Group IV or V positions (energies and structures in Table S2). In contrast to expectations based on NMR, the lowest energy structure (by 0.43 eV) was that with 4 K⁺ in Group V positions and Na⁺ are assigned to Group I, II, III, and IV (as indicated in Scheme 2 for Na-ETS-10 in Table S2). These results suggest K⁺ remains in Group IV positions following Na⁺ washing due to kinetic trapping. As the apertures to access Group IV sites are small in size. Such findings are in accordance with previous work from Anderson et al. [16,32] indicating that Group IV sites were unavailable for ion exchange.

K-ETS-10 contained 16 K cations and 14 Na cations per u.c. (Table 1). The ²³Na 2D 3Q MAS NMR spectrum of K-ETS-10 (Fig. S3a) indicated that Na was present only in Group I and II sites. Combining these results, Na cations were assigned to Group I and II sites, while the remaining sites were covered by K⁺. DFT calculations for structures (Table S2) with possible distributions of 16 K and 16 Na, rounded up from the experimentally determined 14 Na/u.c. indicated that the lowest energy arrangement for K-ETS-10 places 16 K⁺ in Group III, IV, and V, and 16 Na⁺ in Group I and II, in agreement with the NMR results (Scheme 1 for K-ETS-10 in Table S2).

Li-ETS-10 contained 4 K, 15 Na, and 10 Li cations per u.c.. The ²³Na 2D 3Q MAS NMR spectrum of Li-ETS-10 (Fig. S3b) is similar to that for K-ETS-10 (Fig. S3a), corresponding to the presence of Na cations in Group I and II sites [32]. The 4 K cations likely reside in Group IV sites, as they were determined to be kinetically trapped (as discussed above for Na-ETS-10). The Li cations are therefore assigned to Group III and V sites for a total of 12 sites/u.c. (similar to the experimentally determined 10 Li/u.c.). DFT calculations for structures (Table S2) with stoichiometries matching Li-ETS-10 indicate that Group I and Group II sites are occupied by Na, while Group III and Group V sites contain Li. Group IV sites contain K (Scheme 1 for Li-ETS-10 in Table S2). However, consistent with the kinetic trapping of K in Group IV sites, the structure with K in Group V and Li in Group IV is lower energy (by 0.87 eV).

Elemental analysis, ²³Na 2D 3Q MAS NMR, and DFT calculations collectively indicate all ion exchangeable sites of Na-ETS-10 are occupied by a single type of ion, Na⁺, and Na-ETS-10 retains all 32 ions after the washing process. Li and K cations for Li- and K-ETS-10 are present in Group III and V sites that were occupied by Na cations in Na-ETS-10, suggesting that ion-exchange sites in only these two groups participate in the ion exchange of Li and K with Na. We will discuss the exchange affinity of Li⁺ and K⁺ on Na-ETS-10 at low concentration, along with associated DFT results in the following section.

3.3. Quantifying exchange affinity of Li⁺ and K⁺ with Na-ETS-10 at low concentration

Li or K cations were ion exchanged from low concentration aqueous solutions using Na-ETS-10, to understand differences in cation affinity. Figure 5 shows ion exchange isotherms for Li and K with Na from Na-ETS-10, normalized by the mass of Na-ETS-10 (data included in Table S3). $Q_{Li,e}$, the per-solid concentration of Li exchanged with Na-ETS-10 at equilibrium, is plotted as a function of $C_{Li,e}$, the aqueous concentration of Li after ion exchange at equilibrium. At low $C_{Li,e}$, $Q_{Li,e}$ increase linearly with increasing $C_{Li,e}$. At higher $C_{Li,e}$, $Q_{Li,e}$ approaches a constant value. Similar trends are observed for $Q_{K,e}$ as a function of $C_{K,e}$. Notably, at a given $C_{A,e}$ (where A = Li or K), $Q_{K,e}$ is always greater than $Q_{Li,e}$, reflecting a higher exchange affinity. Such isotherms are accurately described by the modified Langmuir equation (Eq. 3) and were used to obtain the equilibrium constant for A-Na exchange ($K_{Li,Na}$ for $K_{Ci,Na}$ for $K_{Ci,Na}$ for $K_{Ci,Na}$ and the theoretical maximum ion exchange capacity ($Q_{Li,max}$ for Li^{+} and $Q_{K,max}$ for $K_{Ci,Na}$).

The equilibrium constant for A-Na exchange ($K_{A,Na}$) and theoretical maximum ion exchange capacity ($Q_{A,max}$) are used to quantify the exchange affinity (Table 3). The values of $K_{A,Na}$ and $Q_{A,max}$ are obtained by fitting experimental data, including $C_{A,e}$, $Q_{A,e}$, and the concentration of Na⁺ at equilibrium for each sample, with the modified Langmuir model (Eq. 3). $K_{K,Na}$ (5.92 ± 0.71) is nearly six times higher than $K_{Li,Na}$ (0.96 ± 0.16), as expected from the greater value of $Q_{K,e}$ than $Q_{Li,e}$ for the same $C_{A,e}$ shown in Figure 5. The differences in slope of the isotherms at lower concentration and clear separation of isotherm plot indicate the higher exchange affinity of K⁺ over Li⁺, implying that a separation of Li⁺ and K⁺ using Na-ETS-10 is achievable. Unlike the significant difference between $K_{K,Na}$ and $K_{Li,Na}$, $Q_{K,max}$ (0.708 ± 0.055 mmol/g) is only slightly higher than $Q_{Li,max}$ (0.824 ± 0.029). The ratio between $Q_{K,max}$ and $Q_{Li,max}$ is similar to the ratio of number of K⁺ exchanged onto K-ETS-10 (12) and the number of Li⁺ exchanged onto Li-ETS-10 (10). However, the calculated numbers of sites required to exchange to attain $Q_{A,max}$ for K and Li onto Na-ETS-10 (7 and 6, respectively) is smaller. Additionally, the fitted $Q_{K,max}$ and $Q_{Li,max}$ are lower than the capacity of a single symmetry Group, consistent with assumptions underlying the modified Langmuir model.

To support our experimental results, we used DFT calculations to determine the free energy change associated with the ion exchange process described in Equation 4. The structure of Na-ETS-10 obtained in Section 3.2, with 4 K⁺ placed in Group IV is used as a starting point to consider cation exchange. To mimic ion exchange at low concentration, we considered the exchange of only one Na⁺ from each of the groups I, II, III, and V with Li⁺ or K⁺, while assuming no K⁺ from exchange group IV participated in the exchange. $E_{\text{Na/A-ETS-10 (s)}}$ and $E_{\text{Na-ETS-10 (s)}}$ were obtained by DFT calculations. However, it is challenging to calculate the chemical potential of ions in solution ($E_{\text{Na^+}}$ (aq_{O}) and $E_{\text{A^+}}$ (aq_{O}) using DFT calculations. Two approaches to overcome this challenge combined DFT calculations with existing tabulated free energy differences based on experimental data [38-41]. Approach 1 adds the measured solvation free energy ($\Delta G_{\text{M^+}}^s$, where M⁺ = K⁺, Na⁺ or Li⁺) to the DFT calculated energies of the gas phase ions, as shown in Equation 5a and as a thermochemical cycle in the supporting information (Figure S2).

$$E_{\mathrm{M}^{+}(aa)} = E_{\mathrm{M}^{+}(a)} + \Delta G_{\mathrm{M}^{+}}^{\mathrm{s}}$$
 Equation 5a

Approach 2 involves the standard reduction potential of solid metal on a hydrogen electrode scale (V_M) , along with a DFT calculation of the solid alkali metal, as represented by Equation 5b. In Approach 2, the reference voltage for the reduction potential becomes irrelevant when calculating exchange energies (Eq. 4), as the difference between the reduction potential of the two cations appears in exchange energies.

$$E_{M^{+}(aq)} = E_{M(s)} + |e| \cdot V_{M}$$
 Equation 5b

The DFT results for single ion exchange are summarized in Table 4. The DFT calculation results for single K⁺ exchange at Group V has favorable exchange energies, consistent with an exchange equilibrium constant greater than 1 (experimentally, Table 3, $K_{K,Na}$ = 5.92 ± 0.71) and greater than that of Li⁺ exchange ($K_{Li,Na}$ = 0.96 ± 0.16). Table 4 reveals a preference for K⁺: Group V >> Group III > Group I > Group II. Such a preference is consistent with findings from Section 3.2 that indicate K⁺ replaces Na⁺ from Group III and V in K-ETS-10. Single Li⁺ exchange results show predominantly positive exchange energies, with values near 0 for Group III, as expected from experimentally assessed $K_{Li,Na}$ values (Table

3) that are approximately unity. Unlike the results of single K⁺ exchange, the DFT calculation results for single Li⁺ exchange contradict with high concentration exchange data and DFT calculation results on Li-ETS-10 from Section 3.2. The single Li⁺ exchange results indicate a preference order: Group III > Group II > Group II > Group II > Group V. This order differs from what was observed for Li-ETS-10, where Li⁺ replace Na⁺ from Group III and V. Despite this, these results indicate that Group III sites are likely to exchange Li⁺. The discrepancy in these findings imply a concentration dependence of exchange energies, suggesting that an expression derived from Langmuir adsorption may not hold for ion exchange at higher cation concentrations. The exchange energy, per Li, calculated for 12 Li exchanging in the high concentration/wash exchanges reported earlier (exchanging 8 Li into Group III and 4 into Group V) can be compared to that predicted by summing 8 Group III and 4 Group V independent exchanges using the data in Table 4. The difference is 0.04 eV per Li ion (0.49 eV total for the 12 ion exchange), suggesting a Langmuir assumption does not full hold, but that differences are small enough to not impact the analysis presented here.

Noteworthy, approaches 1 and 2 are qualitatively consistent, with ΔE values showing the same trends (Table 4). This indicates that despite the fundamental differences in the physicochemical interactions underpinning the two thermochemical cycles, their resultant ΔE values can each be interpreted to similarly describe the complex interactions relevant for aqueous phase ion exchange in small pores. Trends in cation exchange energies, as well as site preferences, observed in DFT calculations are in line with experimental results, despite the significant approximation that cations reside in the ETS-10 pores without any water solvating the positive charges.

4. Conclusions

The ion exchange of Li⁺ and K⁺ using Na-ETS-10 in aqueous solutions was analyzed with a combination of experimental methods and DFT calculations. The maximum exchange capacity of Li⁺ and K⁺ are obtained and the occupancies of ions in modified ETS-10 are examined by ²³Na 2D 3Q MAS NMR spectroscopy and elemental analysis, with the assistance of DFT calculations. The exchange

affinity at low concentration is quantified by fitting the experimental data to the modified Langmuir isotherm. The results demonstrate a distinct favorability for K⁺ exchange over Li⁺ using Na-ETS-10, suggesting the potential of Na-ETS-10 to serve as a separation material in Li⁺ separation process. DFT calculations aided in identifying cation substitution sites, though the apparent kinetic trapping of K⁺ ions in Group IV sites highlights the relevance of kinetic processes, rather than a purely thermodynamic analysis, in considering ion exchange site favorability.

Supporting Information. Experimental data for ion exchange, DFT-derived cation distributions and relative energies, reference powder diffractograms, thermochemical cycle scheme for Approach 1, NMR spectra, and scanning electron micrographs.

Acknowledgments

This work was supported by the National Science Foundation (grant number CBET 2028498).

Prof. James Hodges (PSU) is acknowledged for valuable discussions. We would like to acknowledge

Prof. Robert Rioux (PSU) for access to ICP-OES equipment and Dr. Griffin Canning with other lab

members from Prof. Rioux's lab (PSU) for training and discussions. We thank Dr. Christy George (PSU,

Nuclear Magnetic Resonance Facility) and Dr. Jordan Meyet (PSU) for ²³Na NMR experiments and

discussion. This work used Bridges at Pittsburgh Supercomputing Center and Expanse at San Diego

Supercomputing Center through allocation CTS150057 from the Advanced Cyberinfrastructure

Coordination Ecosystem: Services & Support (ACCESS) program, which is supported by National

Science Foundation grants #2138259, #2138286, #2138307, #2137603, and #2138296.

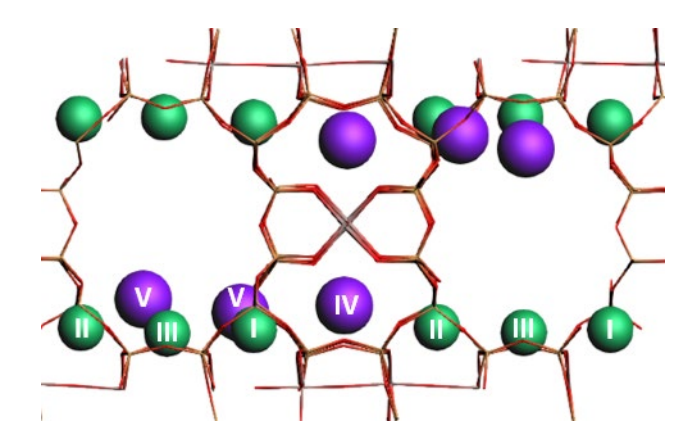


Figure 1. Schematic representation of the five groups of ion exchange sites within the ETS-10 framework. Green and green spheres represent Na^+ and K^+ , respectively, on ion exchange sites. Site occupation is represented for as-synthesized ETS-10.

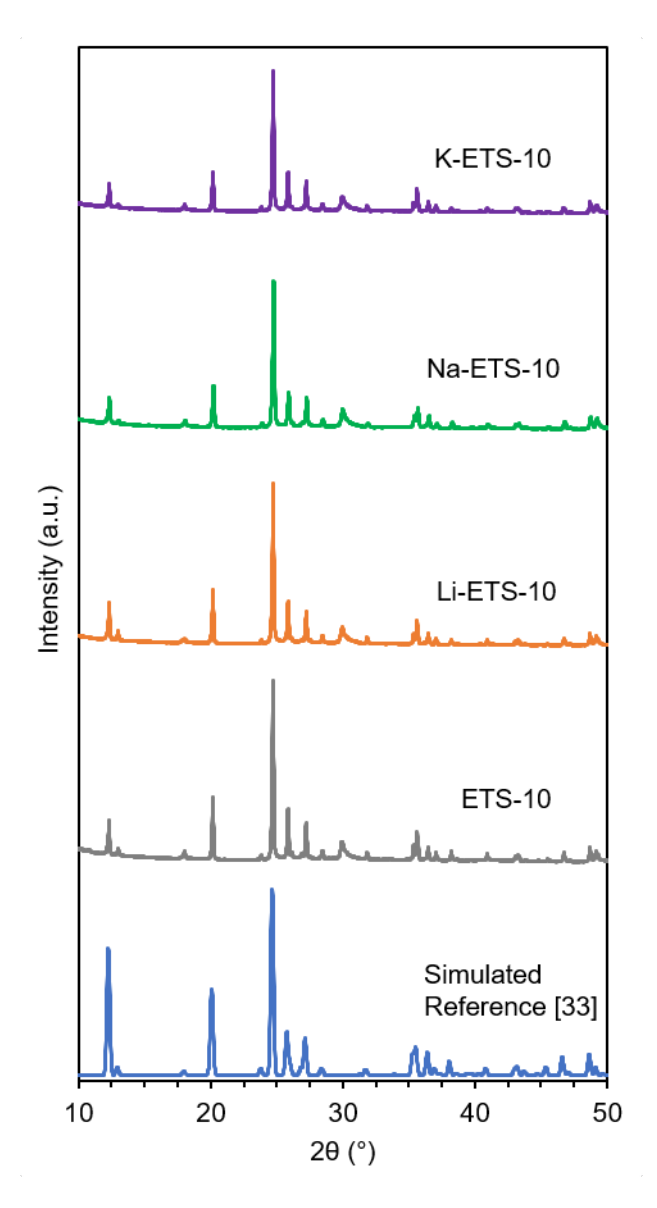


Figure 2. Powder XRD patterns for as-synthesized ETS-10 and washed ETS-10 variants. The simulated powder diffraction pattern is obtained using an experimental single crystal ETS-10 structure [33].

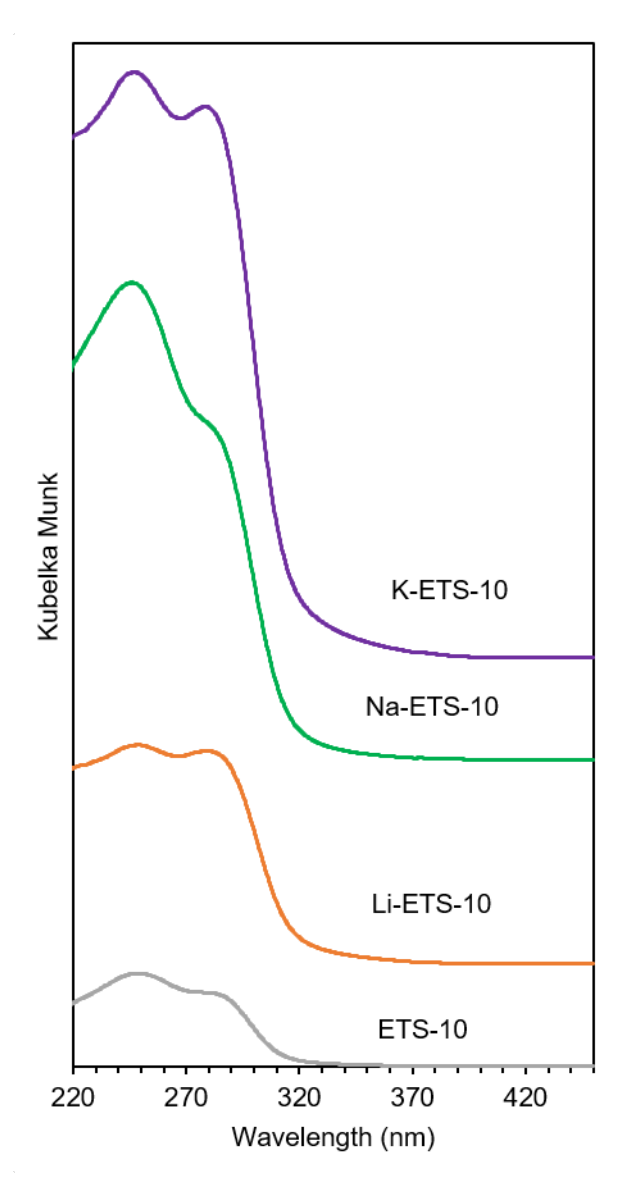


Figure 3. Diffuse reflectance UV-Vis spectra of ETS-10 and washed ETS-10 variants.

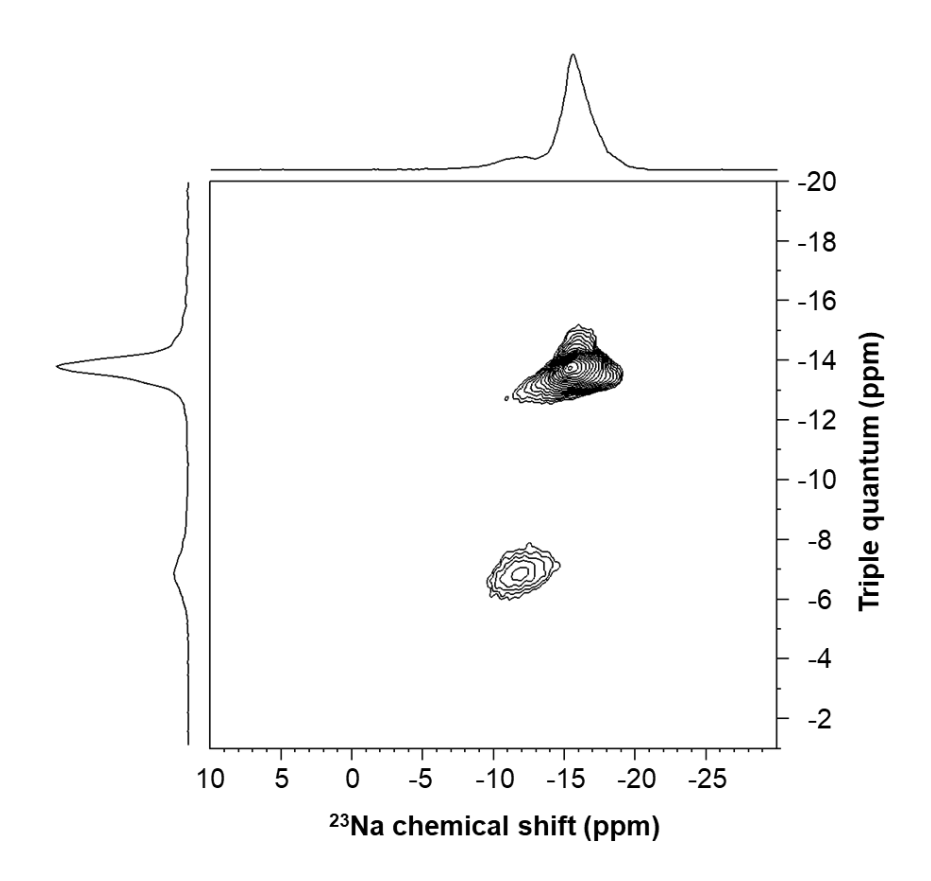


Figure 4. ²³Na 2D 3Q MAS NMR spectrum for Na-ETS-10.

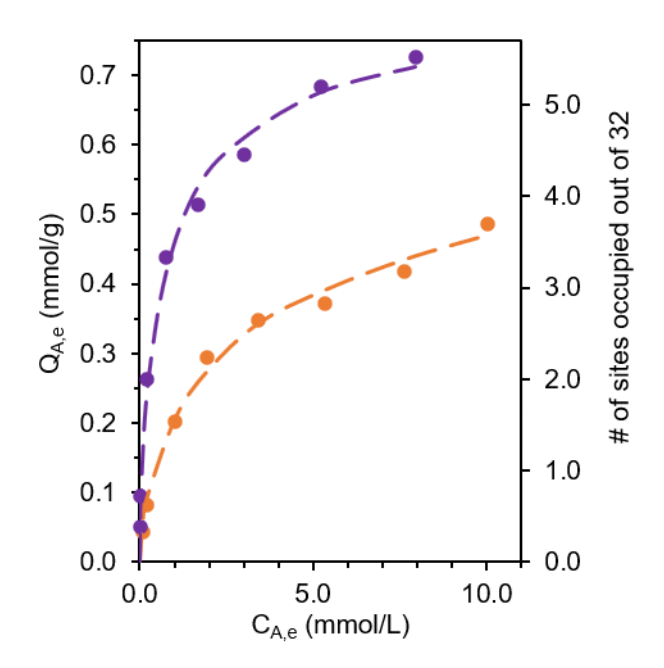


Figure 5. Experimental Li⁺ (orange, \bullet) and K⁺ (purple, \bullet) exchange isotherms with Na-ETS-10 (298 K, 2 h). Dashed lines represent fits to the modified Langmuir isotherm.

Table 1. Elemental composition of ETS-10 and washed variants.

Material	Si/Ti molar ratio	K/u.c.	Na/u.c.	Li/u.c.	Σ(A)/u.c.
ETS-10	4.99	8	24	1	32
K-ETS-10	5.01	16	14		30
Na-ETS-10	4.99	4	28		32
Li-ETS-10	4.96	4	15	10	29

Table 2. Cation configurations for ETS-10 and washed variants, determined based on DFT calculations, elemental analysis, and 23 Na NMR data.

Group Number	I	П	III	IV	V
ETS-10	8 Na ⁺	8 Na ⁺	8 Na ⁺	4 K ⁺	4 K ⁺
Na-ETS-10	8 Na ⁺	8 Na ⁺	8 Na ⁺	4 K ⁺	4 Na ⁺
K-ETS-10	8 Na ⁺	8 Na ⁺	8 K ⁺	4 K ⁺	4 K ⁺
Li-ETS-10	8 Na ⁺	8 Na ⁺	8 Li ⁺	4 K ⁺	4 Li ⁺

Table 3. Equilibrium constant and theoretical maximum Na-ETS-10 exchange capacity for different ions based on the fitting of existing data with the modified Langmuir isotherm model. Error reflects standard error (covariance).

	Equilibrium Constant, K _{A,Na}	Theoretical Maximum Exchange Capacity, Q _{A,max} (mmol/g)
Li	0.96 ± 0.16	0.71 ± 0.06
K	5.92 ± 0.71	0.82 ± 0.03

Table 4. DFT-derived ΔE for ion exchange of one M^+ and Na^+ from Na-ETS-10.

Symmetry Group	M ⁺ , Ion Exchanged	ΔE by Approach 1 (eV)	ΔE by Approach 2 (eV)
Ι	Li	0.22	0.18
II	Li	0.18	0.14
III	Li	0.00	-0.04
V	Li	0.26	0.22
Ι	K	0.31	0.17
II	K	0.35	0.21
III	K	0.10	-0.04
V	K	-0.30	-0.44

References

- 1. U. S. Department of Energy. *Critical Materials Strategy*. 2011. Available at https://www.energy.gov/node/349057 (accessed 2023-06-04).
- 2. U.S. Department of the Interior. *Draft List of Critical Minerals*. 2018. Available at https://www.regulations.gov/document?D=DOI-2018-0001-0001 (accessed 2023-06-04).
- 3. Garside, M. *Projection Total Lithium Demand Globally 2030*. Statista, 2023. https://www.statista.com/statistics/452025/projected-total-demand-for-lithium-globally/ (accessed 2023-06-04).
- 4. Greim, P.; Solomon, A. A.; Breyer, C. Assessment of lithium criticality in the global energy transition and addressing policy gaps in transportation. *Nat. Commun.* **2020**, *11*, 4570.
- 5. Hano, T.; Matsumoto, M.; Ohtake, T.; Egashira, N.; Hori, F. Recovery of lithium from geothermal water by solvent extraction technique. *Solvent Extr. Ion Exch.* **1992**, *10*(2), 195–206.
- 6. Pranolo, Y.; Zhu, Z.; Cheng, C. Y. Separation of Lithium from Sodium in Chloride Solutions Using SSX Systems with LIX 54 and Cyanex 923. *Hydrometallurgy* **2015**, *154*, 33–39.
- 7. Pranolo, Y.; Zhang, W.; Cheng, Y.C. Recovery of metals from spent lithium-ion battery leach solutions with a mixed solvent extraction system. *Hydrometallurgy* **2010**, *102*(1–4), 37–42.
- 8. Zhang, J.; Zhao, B.; Schreiner, B. *Separation Hydrometallurgy of Rare Earth Elements*, p. 259. Springer International Publishing: Switzerland, 2016.
- 9. Kinoshita, K.; Inoue, T.; Fusselman, S. P.; Grimmett, D. L.; Roy, J. J.; Gay, R. L.; Krueger, C. L.; Nabelek, C. R.; Storvick, T. S. Separation of uranium and transuranic elements from rare earth elements by means of multistage extraction in LiCl-KCl/Bi system. *J. Nucl. Sci. Technol.* **1999**, *36*(2), 189-197.
- 10. Brown, C. G.; Sherrington, L. G. Solvent extraction used in industrial separation of rare earths. *J. Chem. Technol. Biotechnol.* **1979**, *29*(4), 193-209.
- 11. Pin, C.; Zalduegui, J. S. Sequential separation of light rare-earth elements, thorium and uranium by miniaturized extraction chromatography: application to isotopic analyses of silicate rocks. *Anal. Chim. Acta* **1997**, *339*(1-2), 79-89.
- 12. Oleksiienko, O.; Wolkersdorfer, C.; Sillanpää, M. Titanosilicates in cation adsorption and cation exchange–a review. *Chem. Eng. J.* **2017**, *317*, 570-585.
- 13. Reck, B. K.; Graedel, T. E. Challenges in metal recycling. *Science* **2012**, *337*(6095), 690-695.
- 14. Hayashi, T.; Yamabe, T. Elution behaviour of the rare earth elements on single and mixed ion-exchange columns. *J. Chromatogr. A* **1973**, 87(1), 227-231.
- 15. Sherry, H. S. The ion-exchange properties of zeolites. I. Univalent ion exchange in synthetic faujasite. *J. Phys. Chem.* **1966**, *70*(4), 1158-1168.
- Anderson, M.; Terasaki, O.; Ohsuna, T.; Malley, P. J. O.; Philippou, A.; Mackay, S. P.; Ferreira, A.; Rocha, J.; Lidin, S. Structure of the microporous titanosilicate ETS-10. *Nature* 1994, 367, 347–351.
- 17. Anderson, M.; Terasaki, O.; Ohsuna, T, Malley, P. J. O.; Philippou, A; MacKay, S. P; Ferreira, A.; Rocha, A.; Lidin, S. Microporous titanosilicate ETS-10: A structural survey. *Philos. Mag. B* **1995**, 71, 813–841.
- 18. Lv, L.; Su, F.; Zhao, X. S. A reinforced study on the synthesis of microporous titanosilicate ETS-10. *Microporous Mesoporous Mater.* **2004**, *76*, 113–122.
- 19. Lv, L.; Tsoi, G.; Zhao, X. S. Uptake equilibria and mechanisms of heavy metal ions on microporous titanosilicate ETS-10. *Ind. Eng. Chem. Res.* **2004**, *43*(24), 7900-7906.
- 20. Yang, X.; Blosser, P. W. Location and bonding of cations in ETS-10 titanosilicate molecular sieve: A multinuclear n.m.r. investigation. *Zeolites* **1996**, *17*(3), 237–243.
- 21. Lv, L.; Su, F.; Zhao, X. S. Incorporation of hybrid elements into microporous titanosilicate ETS-10: An approach to improving its adsorption properties toward Pb2+. *Microporous Mesoporous Mater.* **2007**, *101*(3), 355–362.

- 22. Rahimi, M.; Ng, E. P.; Bakhtiari, K.; Rahimnejad, M.; Samani, F. S.; Amouheidari, M.; Varma, R. S. Zeolite Nanoparticles for Selective Sorption of Plasma Proteins. *Sci. Rep.* **2015**, *5*, 17259.
- 23. Thakkar, J.; Wissler, B.; Dudenas, N. R.; Yin, X.; Vailhe, M. K.; Bricker, J.; Zhang, X. Recovery of critical rare earth elements using ETS-10 titanosilicate *Ind. Eng. Chem. Res.* **2019**, *58*(25), 11121-11126.
- 24. Pavel, C.C.; Popa, K.; Bilba, N.; Cecal, A.; Cozma, D.; Pui, A. The sorption of some radiocations on microporous titanosilicate ETS-10. *J. Radioanal. Nucl. Chem.* **2003**, *258*, 243–248.
- 25. Pavel, C. C.; Popa, K. Investigations on the ion exchange process of Cs+ and Sr2+ cations by ETS materials. *Chem. Eng. J.* **2014**, *245*, 288-294.
- 26. Al-Attar, L.; Dyer, A.; Blackburn, R. Uptake of Uranium on ETS-10 Microporous Titanosilicate. *J. Radioanal. Nucl. Chem.* **2000**, *246*, 451–455.
- 27. Perry, R. H.; Maloney, J. O.; Green, D. W. Adsorption and ion exchange. In *Perry's Chemical Engineering Handbook*; McGraw-Hill: New York, 1984; pp 16-12-16-13.
- 28. Kresse, G.; Furthmüller, J. Efficient Iterative Schemes for Ab Initio Total-Energy Calculations Using a Plane-Wave Basis Set. *Phys. Rev. B* **1996**, *54*, 11169–11186.
- 29. Kresse, G.; Hafner, J. Ab initio molecular dynamics for liquid metals. *Phys. Rev. B* **1996**, 47(1), 558
- 30. Perdew, J. P.; Wang, Y. Generalized gradient approximation made simple. *Phys. Rev. Letters* **1996**, 77(18), 3865.
- 31. Blöchl, P. E. Projector augmented-wave method. *Phys. Rev. B* **1994**, *50*, 17953–17979.
- 32. Anderson, M. W.; Agger, J. R.; Luigi, D.-P.; Baggaley, A. K.; Rocha, J. Cation sites in ETS-10: 23Na 3Q MAS NMR and lattice energy minimization calculations. *Phys. Chem. Chem. Phys.* **1999**, 1(9), 2287–2292.
- 33. Wang, X.; Jacobson, A. J. Crystal Structure of the Microporous Titanosilicate ETS-10 Refined from Single Crystal X-Ray Diffraction Data. *Chem. Commun.* **1999**, *11*, 973–974.
- 34. Rocha, J.; Ferreira, A.; Lin, Z.; Anderson, M. W. Synthesis of microporous titanosilicate ETS-10 from TiCl3 and TiO2: a comprehensive study. *Microporous Mesoporous Mater.* **1998**, *23*(5–6), 253-263.
- 35. Liepold, A.; Roos, K.; Reschetilowski, W.; Lin, Z.; Rocha, J.; Philippou, A.; Anderson, M. W. Characterization studies on the new microporous aluminium-containing ETS-10 molecular sieve used for processing larger molecules. *Microporous Mater.* **1997**, *10*(4–6), 211-224.
- 36. Borello, E.; Lamberti, C.; Bordiga, S.; Zecchina, A.; Areán, C. O. Quantum-size effects in the titanosilicate molecular sieve. *Appl. Phys. Lett.* **1997**, *71*(16), 2319-2321.
- 37. Bordiga, S.; Turnes Palomino, G.; Zecchina, A.; Ranghino, G.; Giamello, E.; Lamberti, C. Stoichiometric and Sodium-Doped Titanium Silicate Molecular Sieve Containing Atomically Defined –Otiotio Chains: Quantum Ab Initio Calculations, Spectroscopic Properties, and Reactivity. *J. Chem. Phys.* **2000**, *112*(8), 3859–3867.
- 38. Kelly, C. P.; Cramer, C. J.; Truhlar, D. G. Aqueous Solvation Free Energies of Ions and Ion—water Clusters Based on an Accurate Value for the Absolute Aqueous Solvation Free Energy of the Proton. *J. Phys. Chem. B* **2006**, *110*(32), 16066–16081.
- 39. Bard, A. J.; Parsons, B.; Jordon, J., Eds. *Standard Potentials in Aqueous Solutions*; Dekker: New York, 1985.
- 40. Milazzo, G.; Caroli, S.; Sharma, V. K. *Tables of Standard Electrode Potentials*; Wiley: London, 1978.
- 41. Swift, E. H.; Butler, E. A. *Quantitative Measurements and Chemical Equilibria*; Freeman: New York, 1972.